

Abstract. Several blazars, and BL Lac objects in particular, show a misalignment between the jet orientation on parsec and kiloparsec scales. Some authors (i.e. Conway & Murphy, 1993) have attempted to explain this behaviour invoking helical jets for misalignment angles around 90° , showing how in this case there are interesting implications for the understanding of the medium into which the jet is expanding. By comparing sensitive VLA observations (Cassaro et al., 1999) with images available in the literature for the BL Lac objects from the 1-Jy Sample (Stickel et al., 1991), it is clear that there is a wide range of misalignments between the initial jet direction and the kpc-scale jet, when detected. We have carried out VLBI observations of these BL Lac objects, in order to investigate the spatial evolution of the radio jets from few tens to hundreds of mas, and to search for helical jets in this class of sources. We present here the first dataset obtained from EVN+MERLIN observations at 5 GHz for seven objects. From these observations we never have a clear detection of helical jets, we only have a possible signature of their presence in 2 objects. In only one of the sources with a misalignment angle around 90° the presence of helical jets can be ruled out. This implies that it is not possible to invoke helical jets to explain the morphology of all the sources showing a misalignment of about 90° between the parsec and the kiloparsec scale jets.

Key words: Galaxies: BL Lacertae objects: general – Galaxies: jets – Radio continuum: galaxies

Bendings of radio jets in BL Lacertae objects

I: EVN and MERLIN observations

P. Cassaro^{1,4}, C. Stanghellini¹, D. Dallacasa³, M. Bondi⁴, and R.A. Zappalà⁴

¹ Istituto di Radioastronomia del CNR, C.P. 141, I-96017 Noto SR, Italy

² Istituto di Radioastronomia del CNR, Via Gobetti 101, I-40129 Bologna, Italy

³ Dipartimento di Astronomia, Università di Bologna, Via Ranzani 1, I-40127, Bologna, Italy

⁴ Dipartimento di Fisica e Astronomia, Città Universitaria, via S. Sofia 78, I-95125 Catania, Italy

Received / Accepted

1. Introduction

While in most radio sources it is possible to see continuity in the direction of the jet, a number of blazars shows large misalignment angles between the jet direction on parsec and kiloparsec scale. The distribution of the misalignment angles (ΔPA), defined as the angle between the parsec and kiloparsec direction of the radio jet has been studied by several authors (i.e. Pearson & Readhead, 1988, Conway & Murphy, 1993, Hong et al., 1998). A comprehensive review on this argument can be found in Appl et al. (1996). They collect the data on 155 sources from six different blazar samples, obtaining a misalignment angle distribution ranging from 0° to 180° . Restricting the study to the BL Lac objects the distribution show an expected peak around 0° , but also a second peak around 90° , harder to explain. Moreover this distribution is lacking in sources with $20^\circ < \Delta PA < 40^\circ$. Hong et al. (1998), have examined the misalignment angles for the blazars selected in the γ -rays by the EGRET experiment, and found that the BL Lac and quasars' ΔPA distributions are different, the quasars being more aligned than the BL Lac objects, with average ΔPA of 21° and 99° , respectively.

Different explanations for the presence of the secondary peak have been proposed. Conway & Murphy (1993) claim that it would be impossible to explain the secondary peak through a simple bend or a double population of simply bent sources, proposing that the jet have a helical trajectory generated by Kelvin-Helmholtz instability, probably induced by precession of the rotation axis of the central black hole or of the accretion disk. Such a mechanism drives the jet in a fixed helical trajectory, a sort of tunnel in which the relativistic plasma is flowing. An alternative is the ballistic jet case, in which different components are emitted from the jet basis following straight paths whose direction depends on the instantaneous direction of the jet basis itself. In the case of a non-ballistic helical jet an interesting role is played by the resonance frequency $\omega^* \simeq 1.3c_{\text{ext}}/R$ (Conway & Wrobel, 1995), which depends on the external (to the jet) sound

speed c_{ext} and on the transversal jet radius, R . This latter, indeed, grows until ω^* is greater than the precession frequency, and becomes constant (saturation) when the two frequencies become comparable. In this phase even the helix amplitude stops growing. In a FR II radio galaxy the intergalactic medium which the jet is going through has a sound speed larger than that required in a FR I, because of the different external density; moreover Bridle & Perley (1984) have determined that the average opening angle of the jets of the FR II is smaller than that of the FR I ones. These considerations lead them to postulate a greater resonance frequency of the gas in a FR II with respect to that of a FR I and hence the saturation of the helical jet would occur sooner in a FR I than in a FR II (Conway & Wrobel, 1995). In principle, this can be useful to distinguish the parent population of the blazar examined, but without adequate statistics it is impossible to use it with some success.

A different mechanism, based on a distortion of the accretion disk, has been proposed by Appl et al. (1996) to explain the misalignment. They have noted that some characteristics of the misalignments, like the lack of connection between the different scales and locally straight parts of the jet, can be compatible with a system of two independent jets, one of which originating in the inner part of the accretion disk, aligned with its rotation axis, and a second one departing from the outer part of the disk having a different rotation axis due to Lense-Thirring precession. Following Appl et al. (1996) the central jet would be the mas-scale jet while the arcsecond scale jet would be that originated from the outer region of the disk. This model could explain the independence of the Doppler factor from the ΔPA . If this is the general scenario, the sources with a small ΔPA would be due to the approximate coincidence of the inner and outer axes.

We observed seven BL Lac objects from the 1-Jy sample (Stickel et al. 1991), with the EVN and the MERLIN at 5 GHz to obtain information on the presence of helical jets on blazars and, if possible, to trace the path of these

jets. Our aim was to image the jet from a few tens to few hundreds of mas and to study the evolution of the jet between the pc and the kpc-scale. Other VLBA data at 1.6 GHz have been obtained and are currently undergoing data processing.

2. Selection of the sample

We have chosen to restrict our research to the BL Lac objects of the 1-Jy sample because in a previous study on extended radio luminosity we have obtained images for most of the sources of this sample with arcsecond resolution (Cassaro et al. 1999). In order to select the objects to observe we derived the distribution of ΔPA of the sources of the 1-Jy sample, through the direct inspection of the available images on the arcsecond and the milliarcsecond-scales. We have been able to determine the ΔPA for 17 objects only, either because the lack of information on the pc-scale, or the difficulty in determining a clear jet or structure on the largest scale. We did not use the values of ΔPA reported in the literature because they are not obtained with a clearly defined and uniform method. We have compared our VLA images (Cassaro et al. 1999) with the images on the pc-scale available in literature and those obtained from the United States Naval Observatory (USNO) Radio Reference Frame Image Database (RRFID, Fey et al., 1996, 1997, 2000). We have determined the ΔPA in the following way: when a clear jet was visible we took the jet axis as the jet direction in pc-scale images, otherwise we considered the straight line connecting the core with the furthest secondary component present in the VLBI image. We considered as kpc-scale direction of the jet the straight line connecting the core and the extended structure (component, elongated halo, jet) nearest to the core, which we believe should be the first region reached by the jet in its path. In the distribution reported in Fig. 1 two depletions are present: the first one, already known, between 45° and 60° , and the second one around 120° , less evident in analogous distributions by other authors (e.g. Appl et al. 1996). Obviously, this latter depletion in our distribution can be due to the poor statistics. We have chosen objects belonging to the three groups recognizable in the figure, that we call A, B, and C according to a $0^\circ < \Delta PA < 45^\circ$, $60^\circ < \Delta PA < 90^\circ$ and $150^\circ < \Delta PA < 180^\circ$ respectively, obtaining the list in Table 1.

3. Observations and data reduction

The radio observations were carried out on 24 November 1998 at 4.99 GHz dual polarization, with an effective bandwidth of 14 MHz, using the European VLBI Network (EVN) and the MERLIN, with the aim to obtain an angular resolution covering structures with angular size ranging from tens to hundreds of mas. The successful EVN antennas for this experiment were Effelsberg, Cambridge, Jodrell Bank (MK2), Medicina, Noto, Onsala,

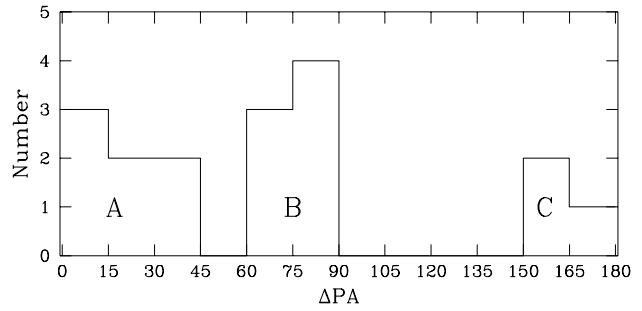


Fig. 1. Distribution of the ΔPA of the 1-Jy sample BL Lacs. It is evident the lack of sources in the intervals 45° - 60° and 90° - 150° .

and Torun. The MERLIN observation made use of the antennas of Defford, Cambridge, Knockin, Darnhall, Jodrell Bank (MK2) and Tabley. Each source was observed for approximately one hour, with short scans distributed at different hour angle to improve the *uv* coverage. The calibration was carried out in a standard way, providing system temperature measurements and gain curves, at the Joint Institute for VLBI in Europe (JIVE) in Dwingeloo (The Netherlands), and the final self-calibration and imaging was performed at the Istituto di Radioastronomia in Noto. We have used the AIPS package for the whole data reduction and analysis.

First, we have obtained the images for the EVN and MERLIN separately and hence, if useful for our aim, we have combined the two datasets to obtain an intermediate resolution image. A small offset ($\leq 10\%$) was found between the amplitudes of the two datasets, as could be determined by comparing the data of the Cambridge-Jodrell baseline, common to both datasets. This offset was corrected accordingly.

4. Images and comments on individual sources

The VLBI images show jet components in good agreement with previous observations. The MERLIN images, instead, have detected emission at a few hundreds of mas from the core in five out of seven objects.

Secondary components are very weak if compared to those on the arcsecond structure, suggesting a high efficiency in carrying the energy at these intermediate scales. In Table 2 we have reported for each source some characteristics of the components on the EVN, MERLIN and (if any) the combined images: in particular the major and minor axis, the distance and the position angle with respect to the core and the flux density. The images are reported in figures 2 through 19. The reference for the arcsecond-scale images of each source is Cassaro et al. (1999), unless otherwise stated.

Table 1. List of the objects observed in this paper. Col. [1] IAU name, col. [2] other name, col. [3] R.A. (J2000) of the pointing center, col. [4] declination (J2000) of the pointing center, col. [5] optical magnitude (Stickel et al. 1991), col. [6] redshift, col. [7] linear size of 1 mas (pc), col. [8] 5 GHz total radio flux, col. [9] misalignment angle (ΔPA), col. [10] group on the misalignment angle distribution (see text).

[1] IAU name	[2] other name	[3] R.A. (J2000) (hh mm ss)	[4] δ (J2000) ($^{\circ}$ ' '')	[5] m	[6] z	[7] l_{1mas} (pc)	[8] S_{5GHz} (Jy)	[9] ΔPA ($^{\circ}$)	[10] group
0814+425	OJ425	08 18 15.999	42 22 45.41	18.5	0.258?	5.0?	>1.69	28	A
0954+658		09 58 47.244	65 33 54.81	16.7	0.367	6.1	1.46	74	B
1147+245	OM280	11 50 19.212	24 17 53.83	16.5	>0.2	>4.2	>1.01	80	B
1308+326	AU Cvn	13 10 28.663	32 20 43.78	19.0	0.997	8.5	1.53	180	C
1418+546	OQ530	14 19 46.597	54 23 14.78	14.5	0.152	3.4	1.09	150	C
1803+784		18 00 45.683	78 28 04.02	16.4	0.684	7.9	2.62	70	B
2131-021	4C-02.81	21 34 10.313	-01 53 17.28	19.0	1.285	8.6	2.12	36	A

0814+425: it is one of the less distorted objects, with a $\Delta PA=28^{\circ}$. The VLBI image (Fig. 2), shows a hint of a jet extended about 10 mas towards the SE direction, confirming previous observations (Polatidis et al., 1995). The MERLIN image (Fig. 3) shows that the jet continues its path for about 100 mas in a direction about 10° bent towards the East. This structure, despite its initial bending, is not a sufficient indication of the presence of a helical jet.

0954+658: this object has a relatively small size, even on the arcsecond-scale. With a $\Delta PA=74^{\circ}$ it belongs to the B group of Fig. 1. The VLBI image (Fig. 4) confirms the presence of a jet in the W-NW direction, slightly resolved, but there are no evident components on the intermediate scale. The weak structure near the core in the MERLIN image (Fig. 5) appears not reliable.

The small size of the source on the arcsecond-scale and the absence of intermediate scale components lead to a jet slightly bent, with a high ΔPA due to projection effects. The lack of (visible) jet at the intermediate scale can be explained by beaming effects: we see the parsec and kpc-scale jet, while the intermediate scale jet is not detectable because it is highly Doppler boosted away from the line of sight.

1147+245: this source has a $\Delta PA=80^{\circ}$, and the jet at the VLBI scale (Fig. 6) is extended about 45 mas towards the West. In the MERLIN image (Fig. 7) a secondary component is present at about 150 mas from the core in the SW direction, at an angle of about 50° from the milliarcsecond-scale jet and 30° from the arcsecond-scale jet. There is no trace of the bending region between the pc-scale jet and the component on the MERLIN scale. The change of direction could be either due to a shock in the interstellar medium or to the passage through a re-

gion where the magnetic field changes direction abruptly (Koide, 1997), or, finally, to a curvature of the jet enhanced by projection effects. Even if we cannot exclude the first two hypotheses, we favour the last one, because of the absence, between the pc scale jet and the secondary component in the EVN+MERLIN image (Fig. 8) of a bright region near to the hypothetical shock in which the jet should dissipate energy and perhaps lose collimation. In Fig. 18 we present radio images of 1147+245 at different angular scales: from left to right our EVN+MERLIN image, the VLA A-array image at 8.4 GHz obtained by Dallacasa et al. (in preparation) and the VLA A+B array image at 1.36 GHz (Cassaro, 2000). The 8.4-GHz VLA image shows that the jet continues to the South then bends sharply toward the SE direction. In the 1.36-GHz VLA image we finally see a double structure with wide jets or maybe lobes where the southern emitting region appears to bend slightly towards the SE direction. The structure is compatible with a helical jet and the abrupt change of direction in the VLBI and VLA 8.4 GHz images would be due to the projection of the helicoid on the plane of the sky.

We note that our images do not cover the scale between $0.15''$ and $0.5''$, that would be important to describe the jet behaviour in the first hundreds of parsec, where we expect to better see the jet behaviour. This angular scale should be adequately covered by the new VLBA data.

1308+326: on the arcsecond scale this source shows a diffuse halo around the core with a luminous region toward the East and a bright pointlike component at about 10 arcseconds toward the North (Murphy et al. 1993). The VLBI image (Fig. 9) shows a jet extended about 10 mas in the W direction, with a ΔPA of 180° or 90° depending on which arcsecond structure we consider as the end of the jet. We favour the first possibility, given that the MERLIN image (Fig. 10) reveals a well-defined

Table 2. Data of the components on the images: col. [1] name of the source; col. [2] image data: “EVN” for VLBI data, “MER” for MERLIN data, “COM” for combined data; col. [3] identity letter of the components, as in the figures; col. [4] and [5] major and minor axis of the component (in mas), if pointlike, “ext” if extended component; col. [6] position angle; col. [7] distance from the core in mas and col. [8] linear projected distance in pc; col. [9] position angle of the component with respect to the core (counted counterclockwise from the north); col. [10] flux density of the component

[1] Name	[2] Data	[3] Comp.	[4] A _{maj} (mas)	[5] A _{min} (mas)	[6] PA (°)	[7] R _{core} (mas)	[8] l _{proj} (pc)	[9] PA _{core} (°)	[10] S _{5GHz} (mJy)
0814+425	EVN	A	5.7	4.8	44	0	0	0	961
		B	7.6	6.6	178	3	16	114	67
	MER	A	48	42	26	0	0	0	899
		B	188.0	60.1	109	97	487	128	12
0954+658	EVN	A	7.0	4.4	145	0	0	0	250
		B	ext	ext	0	12	74	-68	21
	MER	A	48.0	37.5	93	0	0	0	276
		B	ext	ext	0	42	177	102	112
1147+245	EVN	A	11.4	4.5	49	0	0	0	604
		B	ext	ext	0	42	177	102	112
	MER	A	64.3	39.2	135	0	0	0	639
		B	64.0	43.8	139	130	549	-155	26
1308+326	EVN	A	19.1	10.3	31	0	0	0	605
		B	21.0	11.7	36	11	48	-90	58
	MER	C	ext	ext	0	137	580	-163	7
		A	10.5	3.8	35	0	0	0	2216
1418+546	EVN	B	13.7	8.5	54	4	34	-90	112
		MER	A	72.7	40.0	22	0	0	2106
	MER	B	79.2	68.4	51	90	766	-90	14
		C	92.8	48.4	29	230	1958		
1803+784	EVN	A	6.5	4.1	45	0	0	0	409
		B	ext	ext	0	26	89	120	75
	MER	A	50.1	40.1	19	0	0	0	353
		B	67.2	48.9	148	20	68	120	29
2131-021	EVN	C	56.4	35.4	36	130	448	168	2
		A	8.0	4.7	175	0	0	0	1816
	MER	B	8.9	8.3	77	4	32	-92	161
		C	ext	ext	0	50	396	-132	96
COM	MER	A	61.4	39.2	158	0	0	0	1879
		B	71.1	59.8	122	15	119	-81	1879
	EVN	A	13.5	4.3	40	0	0	0	1364
		B	ext	ext	0	23	198	91	135
COM	MER	A	129.9	35.5	20	0	0	0	1358
		B	133.8	47.3	19	11	95	90	238
	EVN	C	129.4	46.0	17	300	2585	180	8
		A	26.2	10.7	18	0	0	0	1358
COM	MER	B	31.0	13.8	19	19	164		
		C	ext	ext	0	138	1189	163	8
	EVN	D	ext	ext	0	226	1947	178	4
		E	ext	ext	0	269	2318	180	2
	EVN	F	ext	ext	0	320	2757	175	3

jet which departs to the West and after about 100 mas bends sharply toward the SW direction, for a total extension of about 200 mas. The jet appears to follow a curved path that encounters the arcsecond-scale East component. In this case the hypothesis of a curvature due to a shock could be considered, but a helical structure

can also easily explain the jet trajectory from mas to the arcsecond-scale.

The observed structures could be also compatible with a mechanism similar to that described for 0954+658. The jet bends smoothly, describing an arc from the mas-scale to the arcsecond-scale, which for projection effects would be visible only in the inner part, becoming

invisible between $0.2''$ and $10''$ in which region the radio emission is boosted away from the line of sight; then it again becomes observable at ~ 10 arcsecond of projected distance from the core at the opposite side of the core, when the velocity of the gas has slowed down and the Doppler factor decreased enough. To verify this scenario it would be important to image the uncovered range of distance from $0.2''$ to about $1''$ - $2''$, to search for possible components of the jet, which, if the latter description is correct, should not be found.

1418+546: in this case $\Delta PA=150^\circ$. The VLBI image (Fig. 11) shows a straight jet directed toward the SE direction. On the intermediate scale (Fig. 12) this source shows a sharp bending perpendicular to the VLBI jet direction. For this source, as in the previous one, the misalignment and the structure are easily explained with a smoothly bending jet, whose curvature is enhanced by the projection.

1803+784: this is the largest object of the 1-Jy sample, with total projected linear size of 444 kpc. In the VLA image a low-brightness region is evident at about 9 arcseconds toward the SW direction with respect to the core; the total radio structure resembles a Wide Angle Tailed (WAT) source. Its ΔPA is 70° and belongs to the second group of Fig. 1. The VLBI image (Fig. 13) shows a collimated jet about 10 mas long which abruptly loses collimation and ends in a diffuse halo slightly bending toward the South, in the direction of the large scale structure. The MERLIN image (Fig. 14) does not reveal any further emission. The extended structure in the image of Fig. 13 could likely be originated by a shock with a denser medium, after which the jet loses collimation and changes its direction towards the arcsecond-scale structure. The enhancement of the apparent bending angle can be due to the projection onto the plane of the sky. The presence of a helical jet for this source is unlikely.

2131-021: we have determined for this source a $\Delta PA=36^\circ$, although in the VLA image different structures can be considered the end of the VLBI jet. In order to determine the misalignment we have taken into account the arcsecond-scale component closest to the core, which presumably will be reached first. The VLBI image (Fig. 15) shows a component in the East direction extended for about 20 mas. In the MERLIN image (Fig. 16) a second component is present toward the South at about 280 mas from the core. The combined image (Fig. 17) shows a jet extended for about 30 mas in the SE direction, and a series of components extending up to 350 mas from the core. The jet appears well collimated, and seems to follow a swinging trajectory, indicating a helical motion. The jet seems collimated and the amplitude of the oscillation constant. If the new VLBA data confirm

this behaviour, it would imply that the saturation takes place in the first tens of mas.

In Fig. 19 we present radio images of 2131-021 at different angular scales: from left to right our EVN+MERLIN image, the VLA A-array image at 8.4 GHz obtained by Dallacasa et al. (in preparation) and the VLA A+B array image at 1.36 GHz (Cassaro, 2000). The 8.4 GHz VLA image shows that the jet axis has a $\sim 45^\circ$ change in its direction while the 1.36 GHz image shows a structure reminiscent of a Narrow Angle Tail (NAT) or a Wide Angle Tail (WAT) radio source. The NAT or WAT classification of this source is also consistent with the change in the direction of the jet axis, which likely occurs at the boundary of the host galaxy.

Even in this case the new VLBA data should cover the scale between $0.35''$ and about $1''$ missing in our images, and would be useful to properly trace the jet and possibly determine the saturation. Moreover, it could be possible to verify where the jet axis changes direction and test the NAT/WAT classification.

5. Discussion and conclusions

EVN+MERLIN observations at 5 GHz have been carried out to investigate the origin of the misalignment between the arcsecond and milliarcsecond-scale structures and to attempt to derive some information from the jet properties on intermediate scale.

A possible explanation for the misalignment, and in particular for the presence of the secondary peak in the ΔPA distribution has been provided by Conway & Wrobel (1995) who consider the presence of a helical jet. Unfortunately, the application of their conclusions has been only possible for Mrk 501, for which the images clearly showed the helical structure and the saturation region. Only two sources observed in this work have morphologies consistent with the presence of a helical jet (1147+245, 2131-021 Figs. 18 and 19). In no case it has been possible to clearly detect a helical jet and it is not possible to determine whether and where the saturation occurs.

Even if there is no sure identification of a helical jet, we can infer some qualitative conclusion from the inspection of our images. The likely helical jets belong to sources with different ΔPA : 80° for 1147+245, 36° for 2131-021. Moreover, in the radio source 1803+784, the strong loss of collimation favours an intrinsic bending due to a shock rather than a helical jet. In summary, one of the sources shows a helical jet structure and do not have a $90^\circ \Delta PA$, and at least one other source with a misalignment of about 90° does not show a helical structure. This suggests that Conway & Murphy's (1993) model, which postulates a population of helical jets to explain the 90° misalignment, may not work for all objects.

Appl et al. (1996) attribute the peak at 90° in the distribution of the misalignments to the presence of two

jets departing from different regions of the accretion disk, without considering any intrinsic distortion of the jet. Several sources examined in this work show characteristics compatible with such a scenario. Some of them, however, show components on intermediate scale (i.e. 2131–021) which do not agree with the presence of only two jets. Moreover some sources have intermediate scale jets that begin to bend, as is the case of 1308+326 and 1418+546. This is in contrast with the conclusions of Appl et al. (1996) who consider straight jets. We note furthermore that such a mechanism can explain the sources with a misalignment around 0° , but cannot do the same with sources belonging to the secondary peak in the misalignment distributions, or better, it cannot explain the lack of BL Lac objects with $45^\circ < \Delta PA < 60^\circ$.

The misalignment distribution of Appl et al. (1996) restricted to the quasars lacks the secondary peak around 90° which is present instead for the BL Lac objects. This suggests that the mechanism that produces the misalignment is likely to be different for these two classes of objects. In particular, for the BL Lacs we can conclude from the images obtained in the present work, that it is unlikely to invoke a single mechanism to explain the misalignment between the arcsecond and milliarcsecond scale structures and the different structures seen in the intermediate scale images.

While a helicoid is not surely proven to be present in all our misaligned sources, a less restrictive hypothesis of non-coplanar bending is required to explain a 90° peak in the distribution. By non-coplanar bending we mean a jet for which the directions in starting and ending regions of the path do not lie in the same plane; a helicoid itself or a branch of a helicoid resulting from a precession motion of only a fraction of a period, are examples of non-coplanar bending. It is also possible to explain the misalignment distribution of the BL Lacs considering that there may co-exist different kinds of objects. A first category with slightly distorted jets, and misalignments distributed from 0° to 180° , with a higher probability of sources with ΔPA around 0° . A second category has misalignments around 90° caused by non-coplanar jets, helical jets or strong ambient interactions (e.g. 1803+784), explaining the numerical excess of BL Lac objects with such a misalignment.

Acknowledgements. The European VLBI Network is a joint facility of European and Chinese radio astronomy institutes funded by their national research councils. MERLIN is operated as a National Facility by the University of Manchester at Jodrell Bank Observatory on behalf of the UK Particle Physics & Astronomy Research Council. The National Radio Astronomy Observatory is a facility of the National Science Foundation operated under cooperative agreement by Associated Universities, Inc.

PC acknowledge the Joint Institute for VLBI in Europe (JIVE) for the support and hospitality during the Summer

Research Program 1999. PC is also very grateful to Denise Gabuzda and Michael Garrett for the very useful help in data reduction.

References

- Appl S., Sol H., Vicente L., 1996, A&A, 310, 419
- Begelman M.C., Blandford R.D., Rees M.J., 1980, Nature, 287, 307
- Bridle A.H., Perley R.A., 1984, ARA&A, 22, 319
- Cassaro P., Stanghellini C., Bondi M., Dallacasa D., della Ceca R., Zappalà R.A., 1999, A&A, 139, 601
- Cassaro P., 2000, PhD thesis, University of Catania
- Conway J.E., Murphy D.W., 1993, ApJ, 411, 89
- Conway J.E., Wrobel J.M., 1995, ApJ, 439, 98
- Fey A. L., Clegg A. W., Fomalont E. B., 1996, ApJS, 105, 299
- Fey A. L., Charlton P., 1997, ApJS, 111, 95
- Fey A. L., Charlton P., 2000, ApJS, 128, 17
- Hong X.Y., Jiang D.R., Shen Z.Q., 1998, A&A, 330, L45
- Koide S., 1997, ApJ, 478, 66
- Murphy D.W., Browne W.A., Perley R.A., 1993, MNRAS, 264, 298
- Pearson T.J., Readhead A.C.S., 1988, ApJ, 328, 114
- Polatidis A.G., Wilkinson P.N., Xu W., Readhead C.S., Pearson T.J., Taylor G.B., Vermeulen R.C., 1995, ApJS, 98, 1
- Stickel M., Fried J.W., Khür H., Padovani P., Urry C.M., 1991, ApJ, 374, 431

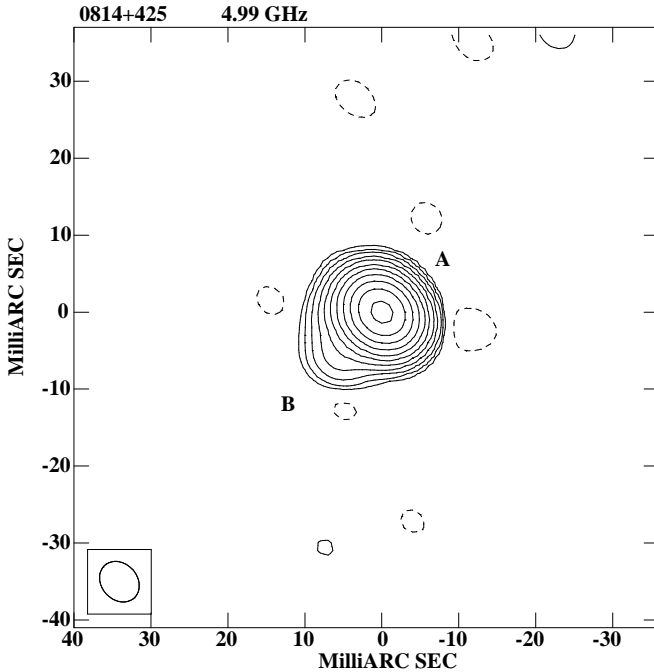


Fig. 2. 0814+425, EVN image. The restoring beam is 5.7×4.6 milliarcsec in PA of 42° . The noise on the image is 0.25 mJy/beam, the contour levels here and in the following figures are $-3, 3 \times 2^i$ ($i=0,1,2,\dots,11$) times the rms noise. The peak flux density is 955 mJy/beam.

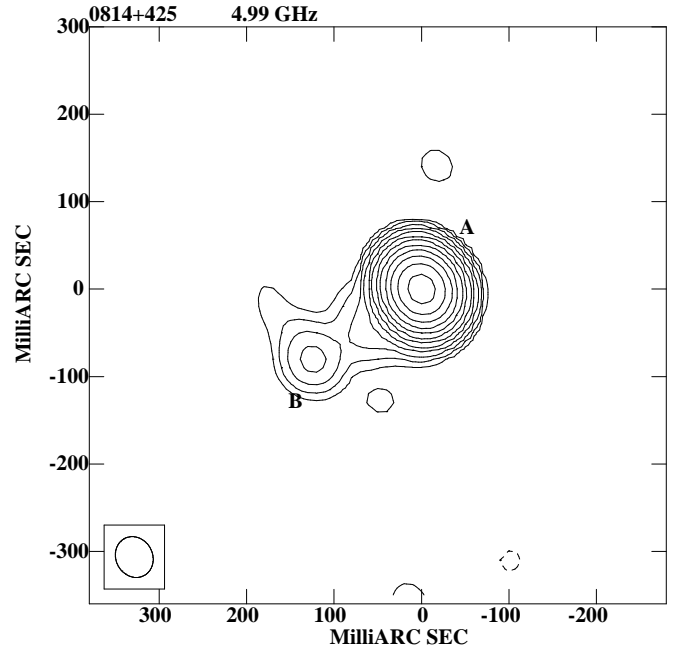


Fig. 3. 0814+425, MERLIN image. The restoring beam is 48×42 milliarcsec in PA of 27° . The noise on the image is 0.1 mJy/beam, the peak flux density is 896 mJy/beam.

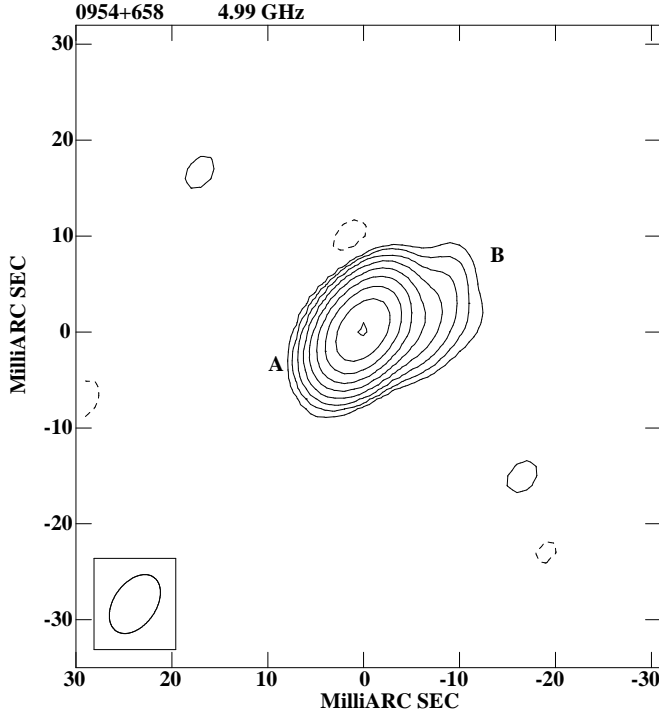


Fig. 4. 0954+658, EVN image. The restoring beam is 6.8×4.4 milliarcsec in PA of -35° . The noise on the image is 0.3 mJy/beam, the peak flux density is 241 mJy/beam.

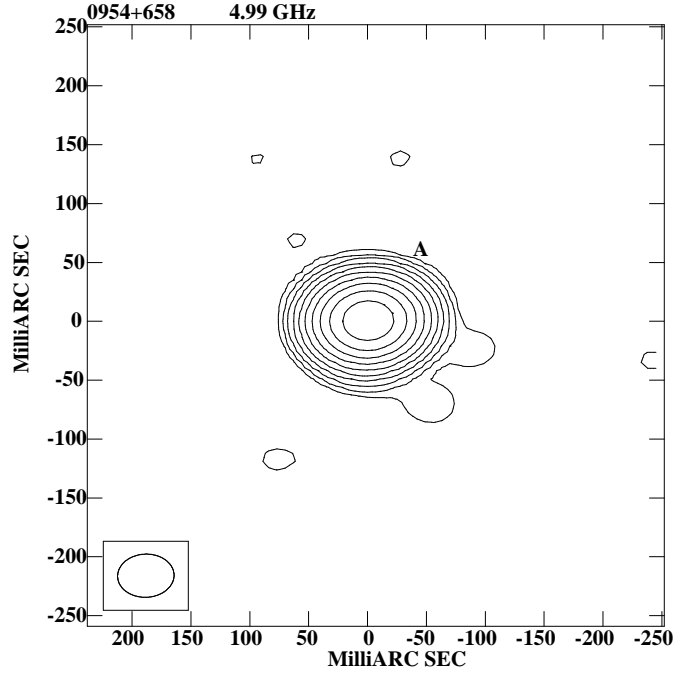


Fig. 5. 0954+658, MERLIN image. The restoring beam is 48×36 milliarcsec in PA of -88° . The noise on the image is 0.1 mJy/beam, the peak flux density is 269 mJy/beam.

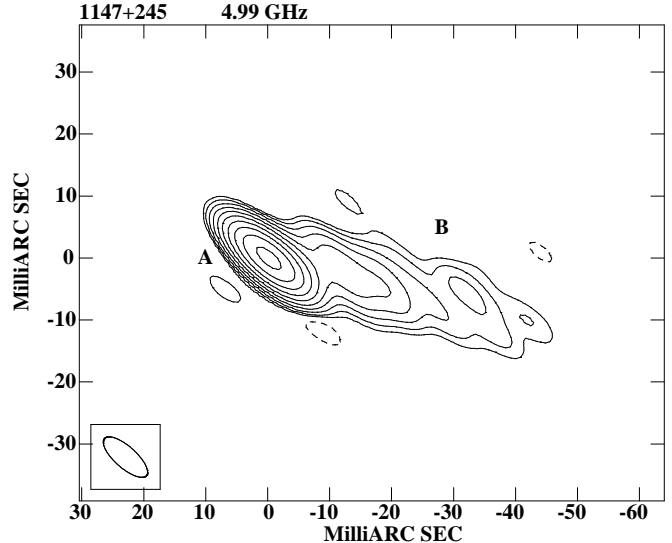


Fig. 6. 1147+245, EVN image. The restoring beam is 9×3.5 milliarcsec in PA of 48° . The noise on the image is 0.3 mJy/beam, the peak flux density is 576 mJy/beam.

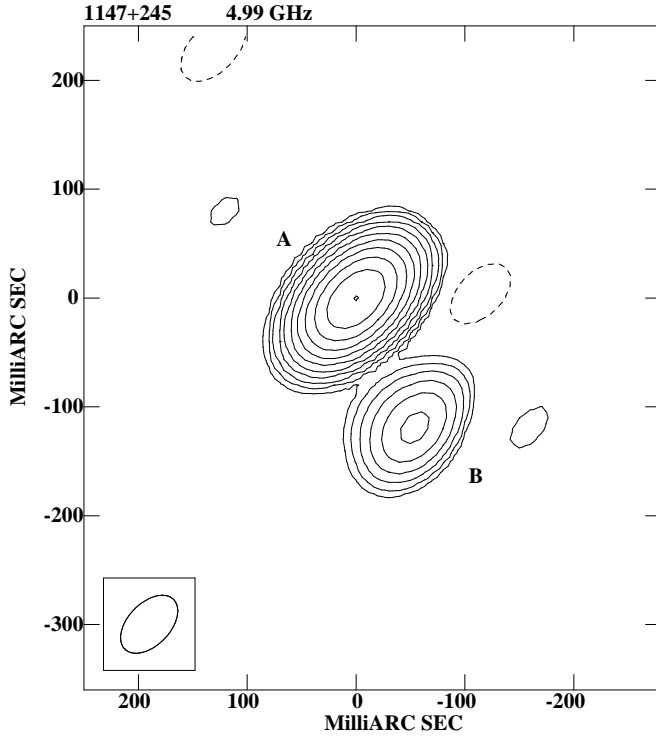


Fig. 7. 1147+245, MERLIN image. The restoring beam is 67×39 milliarcsec in PA of -44° . The noise on the image is 0.2 mJy/beam, the peak flux density is 630 mJy/beam.

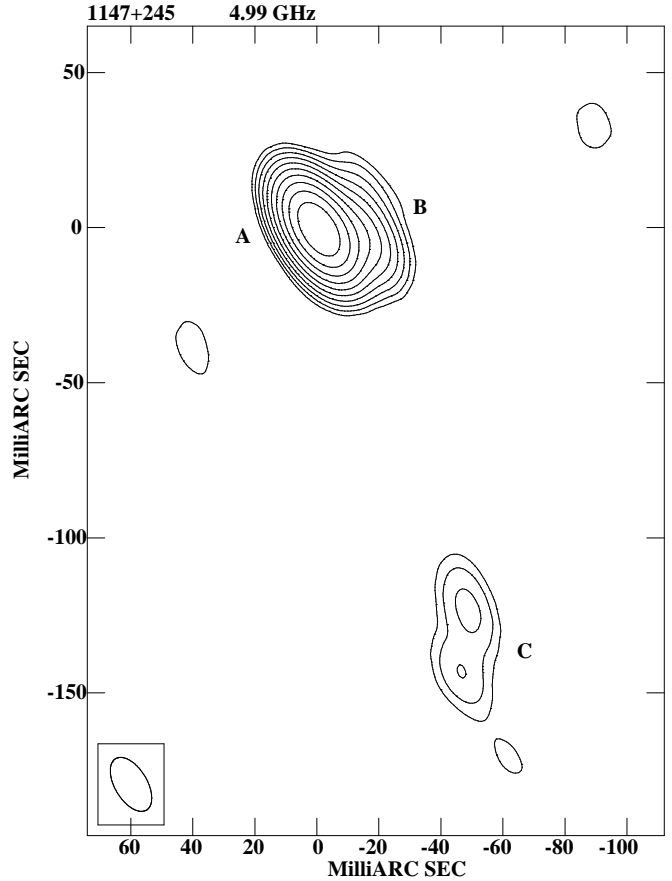


Fig. 8. 1147+245, EVN+MERLIN combined image. The restoring beam is 19×10 milliarcsec in PA of 31° . The noise on the image is 0.2 mJy/beam, the peak flux density is 603 mJy/beam.

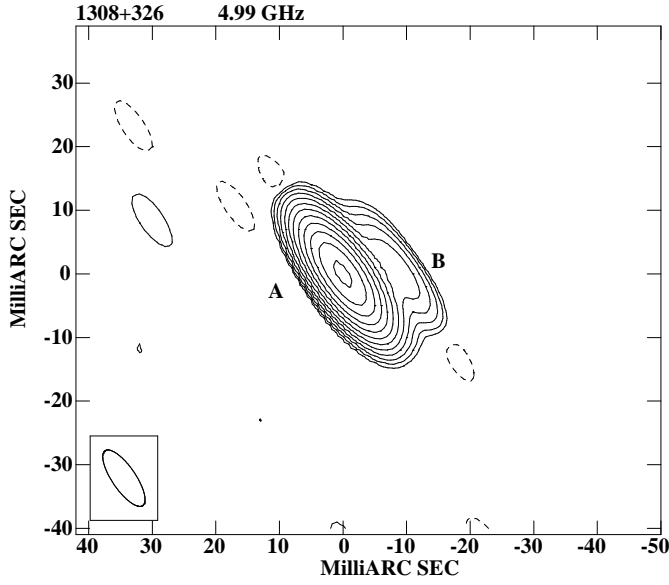


Fig. 9. 1308+326, EVN image. The restoring beam is 10×3.7 milliarcsec in PA of 34° . The noise on the image is 0.3 mJy/beam, the peak flux density is 2170 mJy/beam.

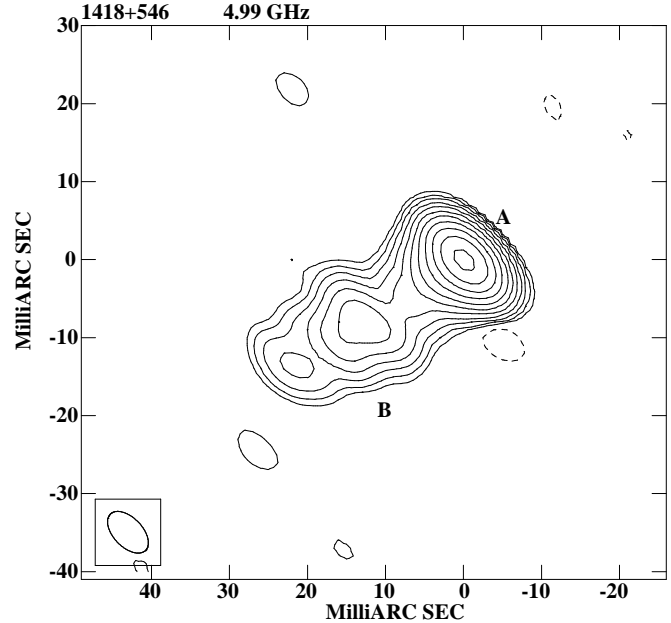


Fig. 11. 1418+546, EVN image. The restoring beam is 6.5×3.7 milliarcsec in PA of 44° . The noise on the image is 0.1 mJy/beam, the peak flux density is 375 mJy/beam.

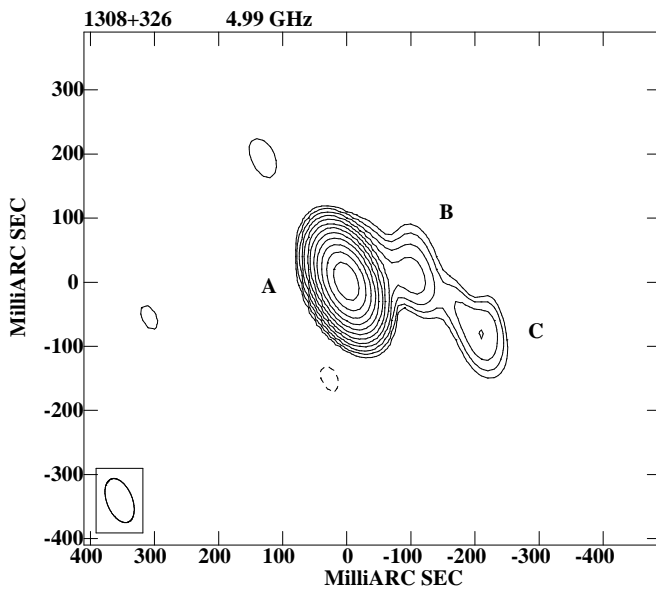


Fig. 10. 1308+326, MERLIN image. The restoring beam is 72×40 milliarcsec in PA of 22° . The noise on the image is 0.2 mJy/beam, the peak flux density is 2075 mJy/beam.

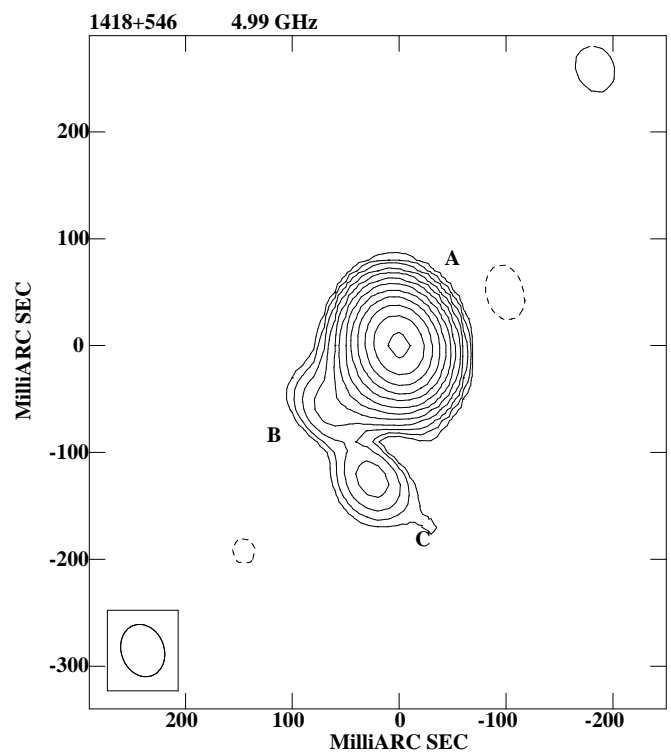


Fig. 12. 1418+546, MERLIN image. The restoring beam is 50×41 milliarcsec in PA of 20° . The noise on the image is 0.05 mJy/beam, the peak flux density is 364 mJy/beam.

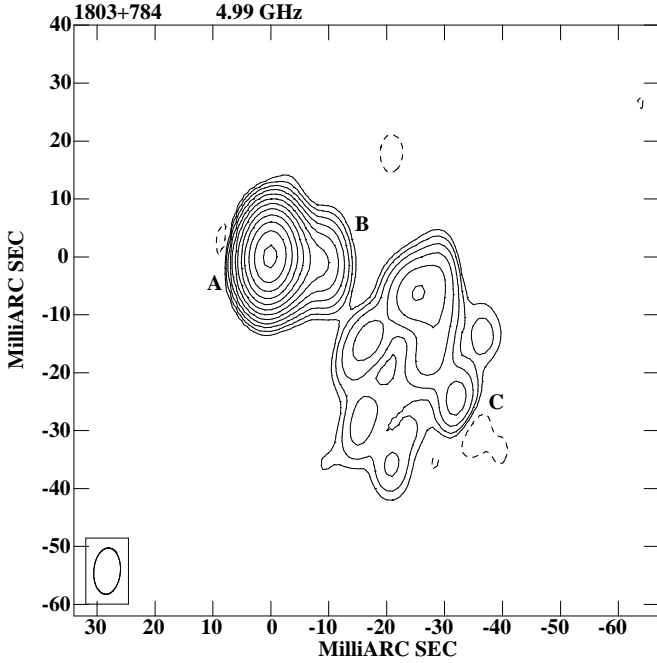


Fig. 13. 1803+784, EVN image. The restoring beam is 8×4.6 milliarcsec in PA of -5° . The noise on the image is 0.25 mJy/beam, the peak flux density is 1819 mJy/beam.

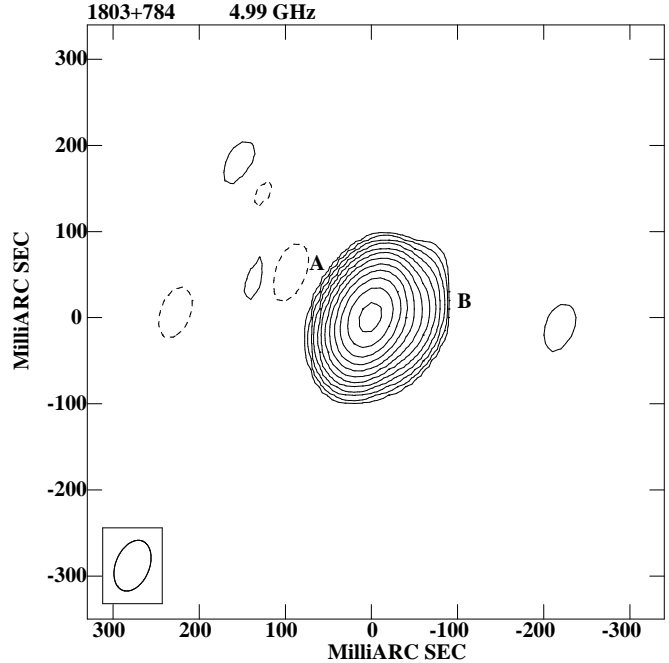


Fig. 14. 1803+784, MERLIN image. The restoring beam is 61×39 milliarcsec in PA of -22° . The noise on the image is 0.25 mJy/beam, the peak flux density is 1989 mJy/beam.

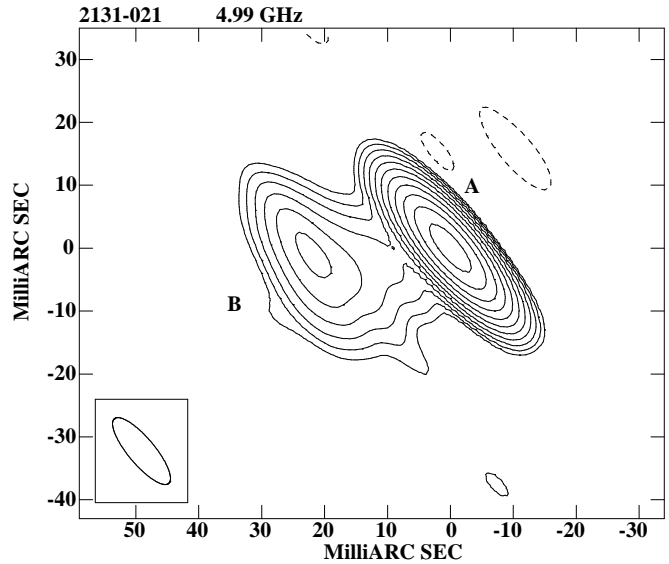


Fig. 15. 2131-021, EVN image. The restoring beam is 13×4.2 milliarcsec in PA of 40° . The noise on the image is 0.3 mJy/beam, the peak flux density is 1341 mJy/beam.

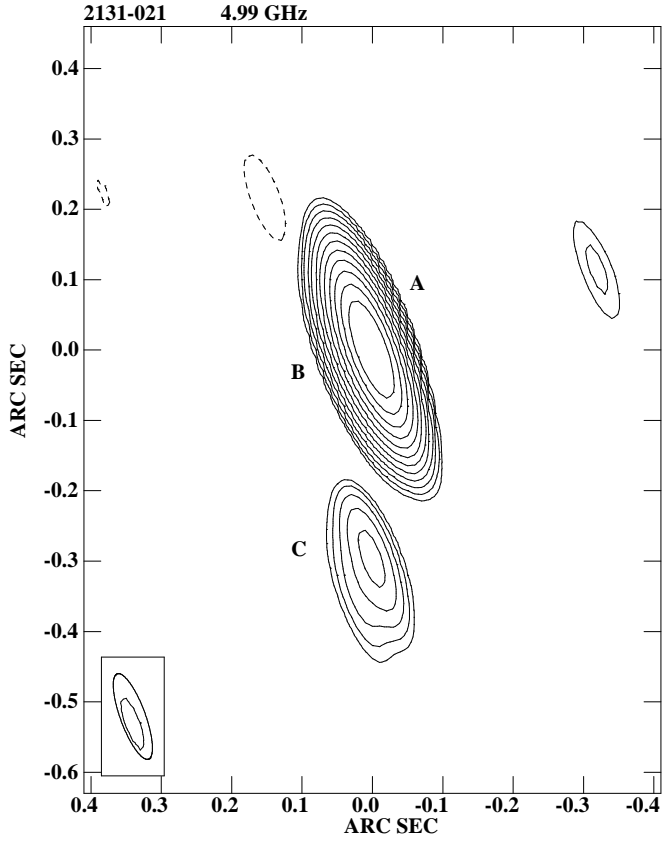


Fig. 16. 2131-021, MERLIN image. The restoring beam is 129×35 milliarcsec in PA of 20° . The noise on the image is 0.1 mJy/beam, the peak flux density is 1509 mJy/beam.

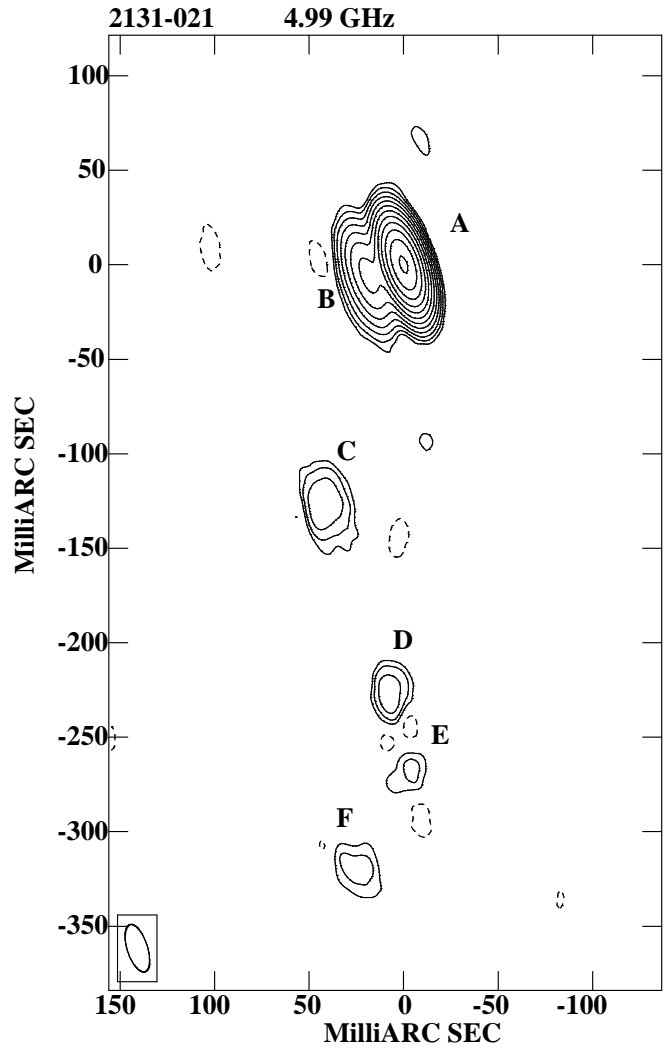


Fig. 17. 2131-021, EVN+MERLIN combined image. The restoring beam is 26×11 milliarcsec in PA of 18° . The noise on the image is 0.2 mJy/beam, the peak flux density is 1349 mJy/beam.

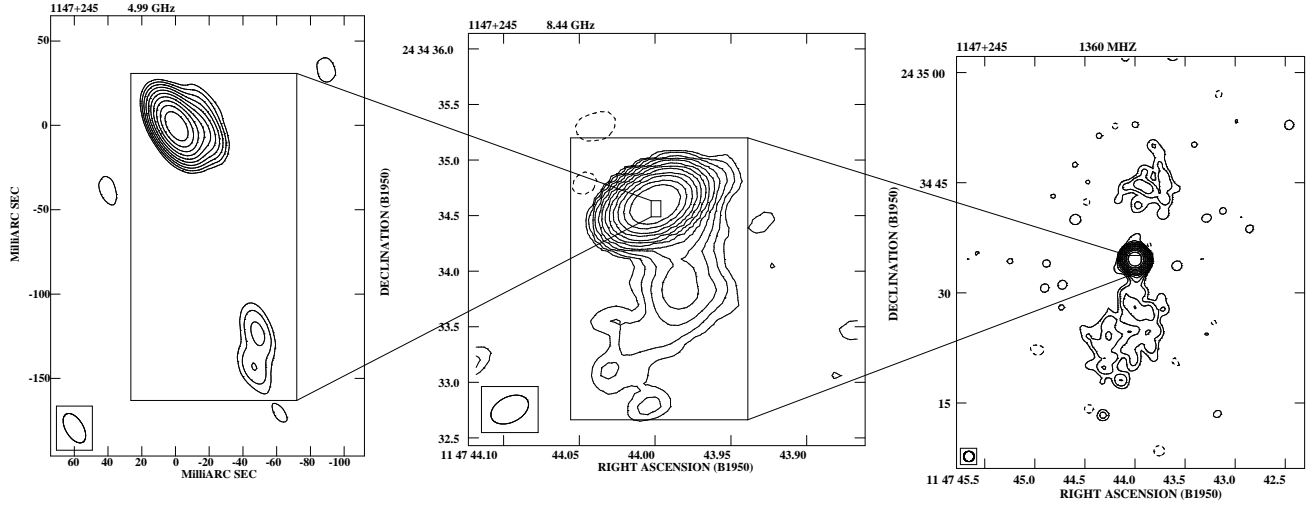


Fig. 18. Comparison of the images at different scales for the source 1147+245. Left panel: EVN+MERLIN combined image (present paper); center panel: VLA A-array image at 8.4 GHz (Dallacasa et al., in preparation); right panel: VLA A+B array combined image at 1.36 GHz (Cassaro, 2000).

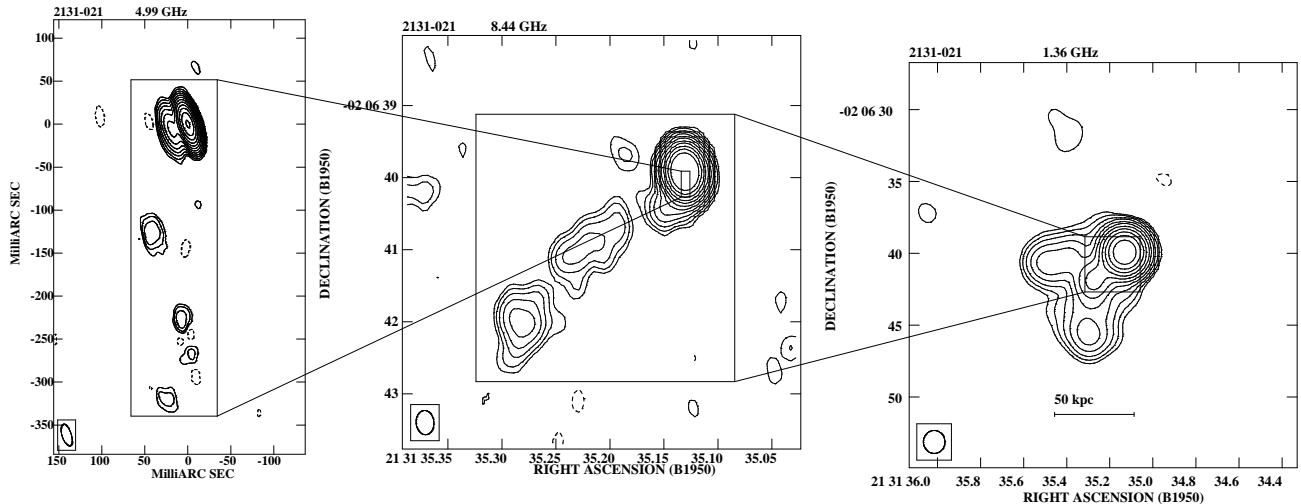


Fig. 19. The same as in Fig. 18 for the source 2131-021. Left panel: EVN+MERLIN combined image (present paper); center panel: VLA A-array image at 8.4 GHz (Dallacasa et al., in preparation); right panel: VLA A+B array combined image at 1.36 GHz (Cassaro, 2000).